Journal of Naval Architecture and Marine Engineering
December, 2023
https://dx.doi.org/10.3329/jname.v20i2.44612 *http://www.banglajol.info*

IMPACT OF CARBON NANOTUBES IN A VERTICAL CHANNEL FOR CASSON FLUID WITH HEAT/MASS FLUX: AN ANALYTICAL STUDY

Silpi Hazarika[1], Sahin Ahmed[2*]
[1]Department of Mathematics, Madhabdev University, Narayanpur, 784164, Assam, India.
Email: silpi.hazarika@rgu.ac.in
[2*]Department of Mathematics, Rajiv Gandhi University, Arunachal Pradesh, India, 791112
Email: sahin.ahmed@rgu.ac.in

Abstract:

This article explores time dependent MHD free convection flow of Casson fluid with carbon nanotubes. The flow is proposed about a vertical channel, and single-wall carbon nanotubes (SWCNTs) and multiple-wall carbon nanotubes (MWCNTs) are placed within the channel with engine oil as base fluid. Modelling the problem is done before applying the perturbation technique to solve it analytically. The computing software Mathematica is used to generate the visual outputs, which are then elaborated for various embedded parameters. It has been established that the Casson parameter and the volume percentage of nanoparticles enhance the flow velocity in both the MWCNT and SWCNT situations. Throughout the discussion, it has become clear that MWCNT outperforms SWCNT for a number of important physical properties. By contrasting the current results with prior literature, a validation of the current work is demonstrated. This work has numerous applications, including in the areas of nanotechnology, hard water, conductive polymers, air refining techniques, mechanical compound materials, superfluous strong filaments, sensing devices, gas storage, biosensors, and many more.

Keywords: *Nanotechnology, CNT's, Casson fluid, magnetic drag force, radiation, nanoparticle volume fraction.*

NOMENCLATURE

$\bar{u}$	dimensional velocity component along x-axis, m/s	R	radiation parameter
$\bar{T}$	Dimensional temperature of the nanofluid, K	Sc	Schmidt number
$\bar{C}$	dimensional concentration of the nanofluid, mol/m^3	t	time, s
u	non-dimensional velocity component along x-axis	d	distance, m
$\bar{T}_0$	temperature at wall $y = 0$, K		**Greek symbols**
$\bar{C}_0$	concentration at wall $y = 0$, mol/m^3	θ	non-dimensional temperature of the nanofluid
$\bar{T}_a$	temperature at wall $y = a$, K	ψ	non-dimensional concentration of the nanofluid
$\bar{C}_a$	concentration at wall $y = a$, mol/m^3	ε	reference constant due to perturbation
B_0	magnetic field strength	σ	electric conductivity, Sm^{-1}
g	acceleration due to gravity	β	Casson parameter
(ρC_p)	heat capacitance, J/K	ρ	density, kg/m^3
Pe	Peclet number	μ	viscosity, kg·m^{-1}·s^{-1}
Re	Reynold's number	κ	thermal conductivity, W/(m·K)
Gr	thermal Grashof number	ω	angular velocity
Gm	mass Grashof number	α	thermal diffusivity, m^2/s
M	magnetic parameter	ϕ	solid volume fraction of nanoparticles

1813-8535 (Print), 2070-8998 (Online) Received on: Dec.,2019

S	suction($S > 0$),	$(\rho\beta)$	thermal expansion coefficient
D	mass diffusivity	γ	Casson parameter
	Subscripts		**Abbreviations**
f	base-fluid	**CNT**	Carbon nanotube
nf	nanofluid	**SWCNT**	Single-wall carbon nanotube
CNT	Carbon nanotube	**MWCNT**	Multi-wall carbon nanotube

1. Introduction

Due to the outstanding relevance in the field of nanotechnology, CNTs have emerged as the dominant technique that has been widely used in the 21st century to boost the rate of heat transfer in many applications. The two types of CNTs that are typically used in nanofluids are single-walled carbon nanotubes (SWCNTs) and multiple-walled carbon nanotubes (MWCNTs). Carbon nanotubes (CNTs) are one of the allotropes of carbon, specifically a class of fullerenes, which are intermediate between buckyballs (closed shells) and graphene (flat sheets). Regarding their structure, characteristics, applications, and forms, carbon nanotubes can be investigated. Casson (1950) designed the Casson fluid, a non-Newtonian fluid model that represents the behaviour of some materials, including suspensions and biological fluids. It is possible to examine complex flows where viscosity varies with applied shear stress using the Casson fluid model since it takes into consideration both shear thinning and yield stress features. Dash (1996) looked into the movement of a Casson fluid in a pipe containing a uniform porous media. The authors described their findings on velocity profiles and pressure drop in the system and gave mathematical modelling and analysis to understand the flow behaviour. Carbon nanotube (CNT) Darcy-Forchheimer flow caused by a revolving disc and a rotating channel was examined by Hayat et al. (2017) and Hussain et al. (2016). A case study of MHD blood flow in a porous media with carbon nanotubes (CNTs) was provided by Khalid et al. (2018) along with a temperature analysis. Also, Khan et al. (2014) looked into the fluid flow and heat transmission of carbon nanotubes (CNTs) along a plate with a Navier slip barrier. The works listed (Kandasamy et al. (2016); Mayer et al. (2013); Pramanik (2014)) cover a variety of topics related to fluid dynamics, heat transfer, and nanofluids. They examine how various nanofluids (SWCNTs, MWCNTs), Casson fluids, and physical phenomena like MHD, heat radiation, porous media, and chemical reactions behave in various flow configurations. These studies aid in the comprehension of complicated fluid systems and shed light on the characteristics of heat transfer and flow behaviour in various contexts. Aman et al. (2017) used four distinct kinds of molecular liquids to study heat transfer enhancement in the free convection flow of carbon nanotubes (CNTs) Maxwell nanofluids. The study's main objective was to examine the thermal behaviour and heat transmission properties of CNT-containing nanofluids. The unstable magnetohydrodynamic (MHD) free convection flow of a Casson fluid via an oscillating vertical plate encased in a porous material was investigated by Asma et al. (2015). While Aman et al. (2017) investigated the impact of a magnetic field on carbon nanotubes' (CNTs') Poiseuille flow and heat transfer down a vertical conduit filled with a Casson fluid. The scientists investigated how a magnetic field affected the flow's behaviour and looked at how it affected the parameters of heat transmission. A study on 3-D channel flow over a porous media was carried out by Ahmed (2009). Beg et al. (2009) investigated the effects of Hall current, ion slip, viscous flow, and Joule heating on unsteady magnetohydrodynamic (MHD) Hartmann-Couette flow and heat transfer in a Darcian channel. In a channel with shape effects, Raza et al. (2019) investigated the MHD flow of molybdenum disulfide nanofluid. Researchers have looked at many facets of fluid dynamics, heat transmission, and nanofluids [Hazarika et al. (2023); Chamkha et al. (2019); Menni et al. (2020); Selimefendigil, et al. (2020)]. They looked explored how various fluids and nanofluids behaved in a variety of flow scenarios, such as those involving magnetic fields, spinning systems, and intricate geometries. This research shed light on the properties of heat transmission, flow behaviour, and the effects of different parameters on nanofluid dynamics. Hazarika and Ahmed's (2021) investigation focuses on the material behaviour of axisymmetric flow in micropolar fluid for heat and mass exchange over a stretchable disc positioned in a porous medium, accounting for the effects of heat generation, diffusion thermo, Brownian motion, and the thermophoretic effect. The flow model is solved numerically by using the MATLAB bvp4c solver. Hazarika et al. (2021) conducted their investigation to gain knowledge about the hydromagnetic flow of a water-based nanofluid containing copper (Cu), silver (Ag), and ferrous ferric oxide (Fe3O4) nanoparticles over a stretching permeable sheet while accounting for heat generation, nanoparticle volume fraction, Soret number, Eckert number, and porosity. In 2022, Hazarika and Ahmed implemented numerical simulation to explore the behaviour of Cu-Water nanofluids on the dual solutions for time-independent, two-dimensional nanofluid flow along a semi-infinite porous stretching horizontal wall in a

porous material for the variation of wall suction/injection and nanoparticle volume fraction and they also used a finite difference numerical tool of the 4th order Runge-Kutta shooting method. Their investigations' unique results could potentially identify areas that still require further research.

The authors aim to understand how the inclusion of carbon nanotubes (both single-wall and multiple-wall) affects the flow behaviour. They investigate the influence of CNTs on the flow velocity and temperature with related parameters. The study aims to explore the effects of key embedded parameters, such as the Casson parameter and nanoparticle volume fraction. By varying these parameters, the researchers wish to determine their influence on the flow characteristics and identify any acceleration or deceleration of the flow velocity. Also, by highlighting the practical implications of the study, the researchers aim to showcase the relevance and significance of their work. The novelty of the article lies in its incorporation of CNTs, analytical solution approach, validation with existing literature, exploration of key physical parameters, and the distinction behaviour of MWCNTs and SWCNTs. These aspects contribute to the advancement of knowledge in the field of unsteady MHD free convection flow and its applications in nanotechnology and related industries.

2. Mathematical Formulation

Here, we take into account an electrically conducting Casson-fluid in a vertical channel (Fig. 1) with width 'a', static walls at $y = 0$ and $y = a$, and a uniform magnetic field with intensity B_0 that is applied transversely to the channel. According to this MHD flow's assumptions, heat and mass are transported by SWCNT and MWCNT and it is presumed to be incompressible and time dependent.

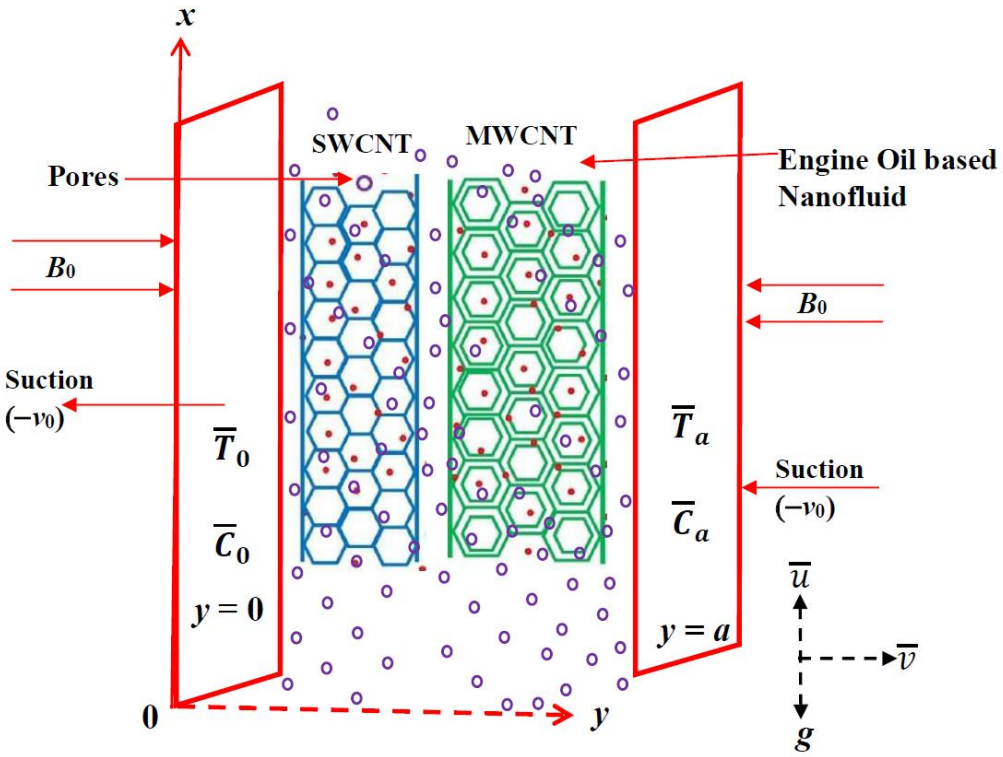

Fig. 1: Physical configuration and coordinate system (Hazarika et al., 2023).

The fundamental modelled equations are (Aman et al., 2017b):

$$\rho_{nf}\left(\frac{\partial \bar{u}}{\partial \bar{t}} + \bar{v}\frac{\partial \bar{u}}{\partial \bar{y}}\right) = \begin{Bmatrix} -\frac{\partial \bar{p}}{\partial \bar{x}} + \mu_{nf}\left(1 + \frac{1}{\gamma}\right)\frac{\partial^2 \bar{u}}{\partial \bar{y}^2} - \sigma_{nf}B_0^2\bar{u} \\ +(\rho\beta)_{nf}g(\bar{T} - \bar{T}_a) + (\rho\beta)_{nf}g(\bar{C} - \bar{C}_a) \end{Bmatrix}, \quad (1)$$

$$\left(\rho C_p\right)_{nf}\left(\frac{\partial \overline{T}}{\partial \overline{t}}+\overline{v}\frac{\partial \overline{T}}{\partial \overline{y}}\right)=-\frac{\partial \overline{q}_r}{\partial \overline{y}}+\kappa_{nf}\frac{\partial^2 \overline{T}}{\partial \overline{y}^2}, \tag{2}$$

$$\left(\frac{\partial \overline{C}}{\partial \overline{t}}+\overline{v}\frac{\partial \overline{C}}{\partial \overline{y}}\right)=D\frac{\partial^2 \overline{C}}{\partial \overline{y}^2} \tag{3}$$

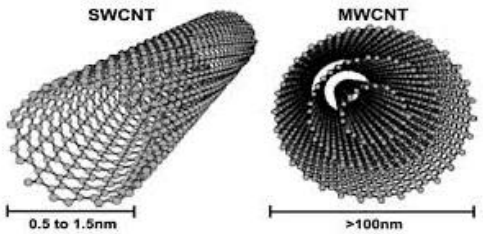

Fig. 2: Distribution of SWCNT and MWCNT.

For nanofluids, the static part in the effective thermal conductivity κ_{nf} and the effective viscosity μ_{nf} are derived from Maxwells (1904), Brinkmans (1952) and Xuan et al. (2003) models and are defined as:

$$\left.\begin{array}{c} \overline{v}=-v_0, \qquad \mu_{nf}=\dfrac{\mu_f}{(1-\phi)^{2.5}}, \ (\rho)_{nf}=(1-\phi)(\rho)_f+\phi(\rho)_{CNT}, \\ (\rho\beta)_{nf}=(1-\phi)(\rho\beta)_f+\phi(\rho\beta)_{CNT}, \ \left(\rho C_p\right)_{nf}=(1-\phi)\left(\rho C_p\right)_f+\phi\left(\rho C_p\right)_{CNT}, \\ \dfrac{\kappa_{nf}}{\kappa_f}=\dfrac{(1-\phi)+2\phi\left(\frac{\kappa_{CNT}}{\kappa_{CNT}-\kappa_f}\right)ln\left(\frac{\kappa_{CNT}+\kappa_f}{2\kappa_f}\right)}{(1-\phi)+2\phi\left(\frac{\kappa_f}{\kappa_{CNT}-\kappa_f}\right)ln\left(\frac{\kappa_{CNT}+\kappa_f}{2\kappa_f}\right)}, \sigma_{nf}=\sigma_f\left[1+\dfrac{3(\sigma-1)\phi}{(\sigma+2)-(\sigma-1)\phi}\right] \end{array}\right\} \tag{4}$$

The radiative heat flux is given by (Aman et al., 2017a):

$$\frac{\partial \overline{q}}{\partial \overline{y}}=-4\alpha^2\left(\overline{T}-\overline{T}_\infty\right) \tag{5}$$

Here are several non-dimensional parameters (Aman et al. 2017b; Hazarika et al., 2023):

$$\left.\begin{array}{c} x=\dfrac{\overline{x}}{d}, \ y=\dfrac{\overline{y}}{d}, \ u=\dfrac{\overline{u}}{U_0}, \ t=\dfrac{\overline{t}U_0}{d}, \ \theta=\dfrac{\overline{T}-\overline{T}_a}{\overline{T}_0-\overline{T}_a}, \ \psi=\dfrac{\overline{C}-\overline{C}_a}{\overline{C}_0-\overline{C}_a}, \\ p=\dfrac{\overline{p}d}{\mu U_0}, \ \omega=\dfrac{\overline{\omega}d}{U_0}, \ \dfrac{\partial p}{\partial x}=\lambda\, exp(i\omega t), \ Re=\dfrac{U_0 d}{\nu_f}, \\ M^2=\dfrac{\sigma_f d^2 B_0^2}{\mu_f}, \ Gr=\dfrac{d^2 g\beta_f(\overline{T}_0-\overline{T}_a)}{U_0\mu_f}, \ Gm=\dfrac{d^2 g\beta_f(\overline{C}_0-\overline{C}_a)}{U_0\mu_f}, \\ R^2=\dfrac{4d^2\alpha^2}{\kappa_f}, \ Pe=\dfrac{U_0 d(\rho C_p)_f}{k_f}, \ \lambda_n=\dfrac{\kappa_{nf}}{\kappa_f}, \ Sc=\dfrac{U_0 d}{D}, \ S=\dfrac{v_0}{U_0} \end{array}\right\} \tag{6}$$

The boundary conditions are (Aman et al., 2017b; Hazarika et al., 2023):

$$\left.\begin{array}{ll} \overline{u}(0,t)=0, & \overline{u}(a,t)=0 \\ \overline{T}(0,t)=\overline{T}_0, & \overline{T}(a,t)=\overline{T}_a \\ \overline{C}(0,t)=\overline{C}_0, & \overline{C}(a,t)=\overline{C}_a \end{array}\right\} \tag{7}$$

The eqns (1) - (3) reduce to the dimensionless form with the aid of (4) - (6):

$$\phi_1 Re\left(\frac{\partial u}{\partial t} - S\frac{\partial u}{\partial y}\right) = \begin{Bmatrix} \varepsilon\lambda exp(i\omega t) + \phi_2\left(1 + \frac{1}{\gamma}\right)\frac{\partial^2 u}{\partial y^2} \\ -M^2\phi_3 u + \phi_4 Gr\theta + \phi_4 Gm\psi \end{Bmatrix}, \tag{8}$$

$$\phi_5 Pe\frac{1}{\lambda_n}\left(\frac{\partial\theta}{\partial t} - S\frac{\partial\theta}{\partial y}\right) = \frac{\partial^2\theta}{\partial y^2} + \frac{R^2}{\lambda_n}\theta, \tag{9}$$

$$\left(\frac{\partial\psi}{\partial t} - S\frac{\partial\psi}{\partial t}\right) = \frac{1}{Sc}\frac{\partial^2\psi}{\partial y^2} \tag{10}$$

The forms of (7) in non-dimensions are

$$\begin{Bmatrix} u(0,t) = 0, & u(1,t) = 0 \\ \theta(0,t) = 1, & \theta(1,t) = 0 \\ \psi(0,t) = 1, & \psi(1,t) = 0 \end{Bmatrix} \tag{11}$$

Rewriting the equations (8) - (10) as

$$a_0\left(\frac{\partial u}{\partial t} - S\frac{\partial u}{\partial y}\right) = \varepsilon\lambda exp(i\omega t) + a_1\frac{\partial^2 u}{\partial y^2} - a_2 u + a_3\theta + a_4\psi, \tag{12}$$

$$b_0\left(\frac{\partial\theta}{\partial t} - S\frac{\partial\theta}{\partial y}\right) = \frac{\partial^2\theta}{\partial y^2} + b_1\theta, \tag{13}$$

$$\left(\frac{\partial\psi}{\partial t} - S\frac{\partial\psi}{\partial y}\right) = \frac{1}{Sc}\frac{\partial^2\psi}{\partial y^2} \tag{14}$$

The perturbed solutions of the equations (12)-(14) with boundary conditions (11) are supposed to have the following forms:

$$F(y,t) = F_0(y) + \varepsilon\, e^{i\omega t}F_1(y), \tag{15}$$

where F stands for $u, \theta \; or \; \psi$.

Equation (15) are incorporated into equations (12)- (14) to form the following system of ODEs:

$$\frac{d^2u_0(y)}{dy^2} + a_9\frac{du_0(y)}{dy} - a_5u_0(y) = -a_6\theta_0(y) - a_7\psi_0(y), \tag{16}$$

$$\frac{d^2u_1(y)}{dy^2} + a_9\frac{du_1(y)}{dy} - a_8u_1(y) = -\lambda_1 - a_6\theta_1(y) - a_7\psi_1(y), \tag{17}$$

$$\frac{d^2\theta_0(y)}{dy^2} + b_2\frac{d\theta_0(y)}{dy} + b_1\theta_0(y) = 0, \tag{18}$$

$$\frac{d^2\theta_1(y)}{dy^2} + b_2\frac{d\theta_1(y)}{dy} - b_3\theta_1(y) = 0, \tag{19}$$

$$\frac{d^2\psi_0(y)}{dy^2} + d_0\frac{d\psi_0(y)}{dy} = 0, \tag{20}$$

$$\frac{d^2\psi_1(y)}{dy^2} + d_0\frac{d\psi_1(y)}{dy} - d_1\psi_1(y) = 0 \tag{21}$$

The converted boundary conditions (11) are:

$$\begin{Bmatrix} u_0(0)=0\,, & u_0(1)=0\,, & u_1(0)=0\,, & u_1(1)=0 \\ \theta_0(0)=1\,, & \theta_0(1)=0\,, & \theta_1(0)=0\,, & \theta_1(1)=0 \\ \psi_0(0)=1\,, & \psi_0(1)=0, & \psi_1(0)=0\,, & \psi_1(1)=0 \end{Bmatrix} \tag{22}$$

The solutions to the equations (16) to (21) under boundary conditions (22) lead to

$$u(y,t)=\begin{bmatrix} \{(p_5-D)e^{-n_3y}+De^{n_3y}+p_1e^{-n_2y}-p_2e^{n_2y}+p_3-p_4e^{-d_0y}\} \\ +\varepsilon e^{(i\omega t)}\left\{-\left(E+\frac{\lambda_1}{a_8}\right)e^{-n_4y}+Ee^{n_4y}+\frac{\lambda_1}{a_8}\right\} \end{bmatrix} \tag{23}$$

$$\theta(y,t)= Be^{-n_2y}+(1-B)e^{n_2y} \tag{24}$$

$$\psi(y,t)=A+(1-A)e^{-d_0y} \tag{25}$$

3. Validity and Accuracy

By contrasting the outcomes with those published by Aman et al. (2017b) for $Gm=0$ and $Gm=2$ for velocity, the accuracy of the current model of SWCNT and MWCNT is confirmed. The velocity comparison for SWCNT-Engine oil is shown in Tables - 1.

Table – 1: Velocity Distribution for Gm in SWCNT for Engine oil at $\lambda=1, t=2, \omega=2, R=2, Gr=0.5, Re=2, Pe=3.5, Sc=2, S=2, M=2$.

Aman *et al.* (2017b) at $Gm=0$				**Present work at $Gm=2$**		
y	**γ = 0.5**	**γ = 1.0**	**γ = 1.5**	**γ = 0.5**	**γ = 1.0**	**γ = 1.5**
0.0	0	0	0	0	0	0
0.2	0.4332	0.6087	0.6998	1.0039	1.4091	1.6198
0.4	0.4106	0.5381	0.5918	0.9731	1.2701	1.3949
0.6	0.2810	0.3458	0.3650	0.6608	0.8006	0.8374
0.8	0.1392	0.1641	0.1683	0.3151	0.3555	0.3532
1.0	0	0	0	0	0	0

In both the $Gm=0$ and $Gm=2$ situations for SWCNT, Table 1 demonstrates that the velocity rises as Gm raises. The outcomes demonstrate that the approach offers highly accurate and excellent approximations to the analytical solution of nonlinear systems.

4. Results and Discussion

SWCNT and MWCNT have been employed with engine oil as the base fluid for all the flow velocity and fluid temperature graphs in this inquiry, where nanoparticle volume fraction is taken as $\phi=0.05$. The default parameters are $\lambda=1, R=2, Gr=0.5, Re=2, Pe=3.5, Sc=0.78, S=2, M=2$.

Table – 2: Thermophysical properties of Engine oil and CNTs (1904).

	$\rho(Kg/m^3)$	$C_p(J/KgK)$	$k(W/mk)$	$\sigma(S/m)$	$\beta\times10^5(K^{-1})$
Engine oil	884	1910	0.144	0.8	0.18
SWCNT's	2600	425	6600	10^6-10^7	27
MWCNT's	1600	796	3000	1.9×10^{-4}	44

As can be shown in Fig. 3, the Casson parameter enhances flow velocity in both the SWCNT and MWCNT situations. The Casson parameter is frequently used to explain the rheological behaviour of complicated fluids, which includes some varieties of nanofluids such SWCNT and MWCNT. The Casson parameter represents the fluid's yield stress and establishes the flow properties in the setting of CNTs. Furthermore, buoyancy forces result

in maximum peak values, which raise the flow velocity in the middle of the channel. The fluid velocity is also accelerated by the Solutal parameter. Throughout the action, MWCNT is evidently more dominating than SWCNT. The shear-thinning effect intensifies with increasing Casson parameter. As a result, at greater shear rates, the fluid's viscosity falls more quickly, facilitating the flow of the CNT suspension and resulting in higher velocities.

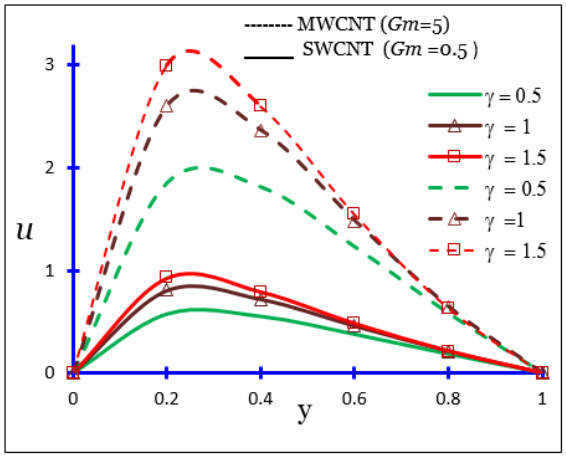

Fig. 3: Velocity distribution of Casson parameter (γ) for MWCNT ($Gm = 5$) and SWCNT ($Gm = 0.5$).

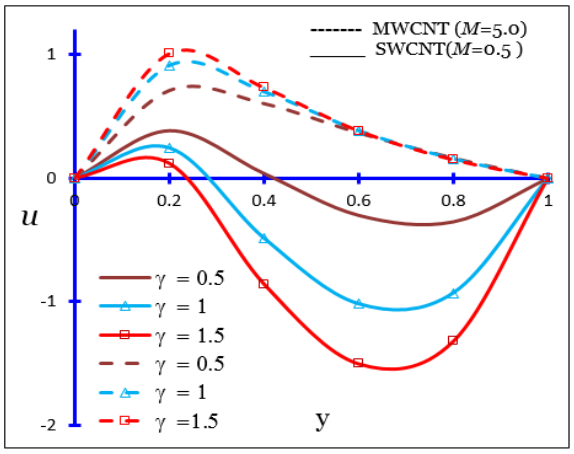

Fig. 4: Velocity distribution of Casson parameter (γ) for MWCNT ($M = 5$) SWCNT ($M = 0.5$).

Fig. 4 depicts the impact of the Casson parameter and the magnetic parameter. While the flow velocity is increased in a negative sense at the lower $M = 0.5$, the Casson parameter enhances the nanofluid velocity in CNTs at the higher $M = 5.0$. Additionally, the larger magnetic field ($M = 5.0$) in MWCNT overpowers the smaller magnetic field ($M = 0.5$) in SWCNT, and intriguingly, the velocity of the large magnetic field from SWCNT to MWCNT is accelerated. Due to the negative velocity in the channel's middle, back flow has occurred. MWCNTs interact hydrodynamically with the surrounding fluid and other particles when a magnetic field is present. These interactions can produce backflow and negative velocities by causing vortices, regions of recirculation, or flow instabilities. The nanoparticles by MWCNTs may move against the main flow direction as a result of the interaction between hydrodynamic and magnetic forces, which can alter the predicted flow behaviour.

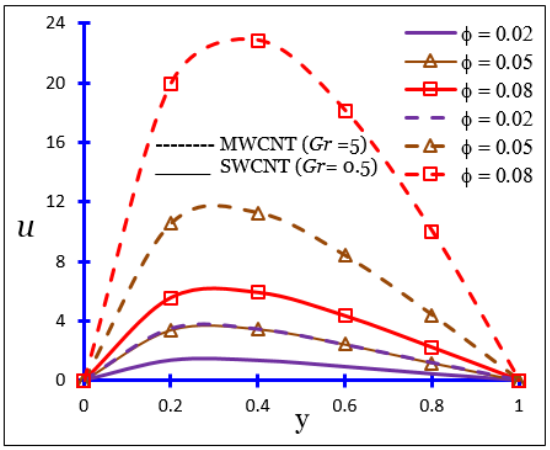

Fig. 5: Velocity distribution of nanoparticles volume fraction (ϕ) for MWCNT ($Gr = 5$) an d SWCNT ($Gr = 0.5$).

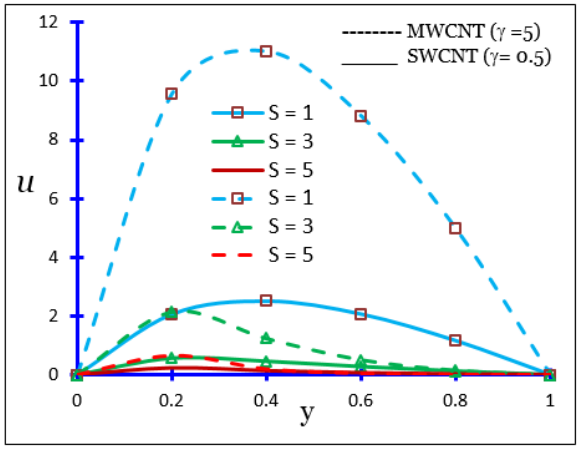

Fig. 6: Velocity distribution of suction (S) for MWCNT (γ=5) and SWCNT (γ =0.5).

Fig. 5 shows the impact of the free convection parameter and nanoparticle volume fraction on the fluid velocity. However, the stronger buoyancy force always accelerates the flow pattern. In this instance, ϕ and Gr lifted all the

profiles of velocity and reached their greatest value in the center of the channel. For the effect of Gr, MWCNT predominates over SWCNT throughout the motion. Increased drag reduction may result from the presence of nanoparticles in the CNT solution. More particles are disseminated within the fluid as the volume fraction of nanoparticles rises. These nanoparticles can interact with the fluid around the CNTs and change how the flow behaves. The fluid can flow more freely through the channel when there are nanoparticles present because they can lessen the fluid's total drag. Due to the lower flow resistance, the velocity of the CNTs rises with increasing nanoparticle volume percentage.

Casson parameter (γ) and suction/injection parameter (S) impacts on fluid velocity are shown in Fig. 6. The fluid velocity declines with an increase in S in both the situations of SWCNT and MWCNT. Due to the high heat conductivity and the lowest values of γ, it can be seen that the corresponding profiles of u in SWCNT thicken. The fluid's effective viscosity may rise as a result of wall suction in the vicinity of the channel walls. The residual fluid encounters a higher CNT concentration when fluid is withdrawn, which contributes to increased viscosity. The increasing viscosity causes more viscous resistance to flow, which lowers the CNTs' speeds. The wall suction controls the resistance and slows the particle flow.

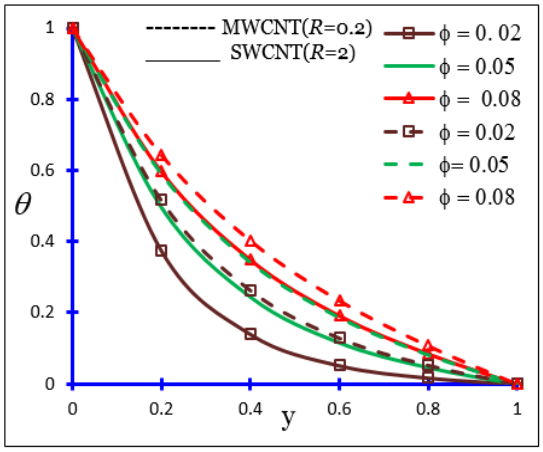

Fig. 7: Temperature distribution of nanoparticles volume fraction (ϕ) for MWCNT ($R = 5$) SWCNT ($R = 2$).

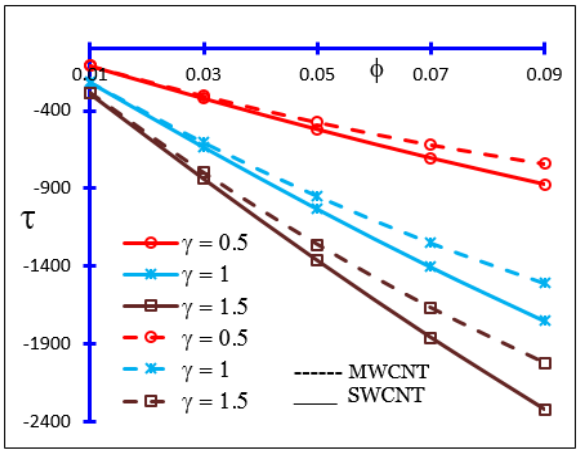

Fig. 8: Shear stress distribution of nanoparticles volume fraction (ϕ) and Casson parameter (γ) for MWCNT and SWCNT.

In Fig. 7, the fluid temperature rises in both the SWCNT and MWCNT situations due to the nanoparticle volume fraction and thermal radiation. While the minimum temperature in SWCNT occurred at $R = 2.0$ and the thermal boundary layer thickness boosted the maximum temperature in MWCNT was found at $R = 0.2$. Excellent thermal conductivity qualities can be found in CNTs. The volume percentage of nanoparticles grows together with the concentration of CNTs in the fluid. The effective thermal conductivity of the fluid is increased as a result of the higher concentration. The fluid's temperature rises as a result of the improved thermal conductivity's capacity for more effective heat transmission. Thermal radiation is the term used to describe the transport of heat by electromagnetic waves created by the fluid around the CNTs. Thermal radiation is emitted by the CNTs and fluid as their temperatures rise. An extra mechanism for transferring energy inside the system may be provided by this radiative heat transfer. The temperature of the fluid drops as the thermal radiation rises because more heat is lost from the fluid as a result.

The impacts of γ and ϕ on the shear stresses has portrayed in Fig. 8. The shear stress develops negative throughout the motion in Casson fluid and it designates that back flow has been observed. The nanoparticle volume fraction and Casson parameter reduce the shear stress substantially. It has been perceived that the MWCNT is followed by SWCNT. The fluid's effective viscosity may rise in the presence of nanoparticles like CNTs. The effective viscosity of the mixture rises as the volume percentage of nanoparticles rises because more nanoparticles are scattered throughout the fluid. A fluid with a higher viscosity will likely have more internal friction, which will cause more shear stresses as the fluid moves through the channel. The addition of CNTs increases the fluid's overall viscosity and contributes to the fluid's increased shear stresses.

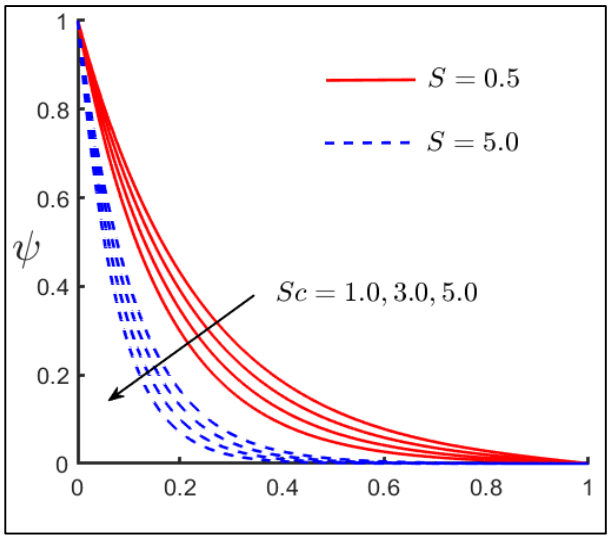

Fig. 9: Concentration distribution of Schmidt Number for $S = 5$ and $S = 0.5$.

Fig. 9 illustrates the dual effects of suction and Schmidt number. The Schmidt number is a dimensionless variable that connects a fluid's mass diffusivity to its momentum diffusivity (viscosity). A lower mass diffusivity compared to momentum diffusivity is indicated by a greater Schmidt number. This suggests that species diffusion happens less efficiently in the fluid than momentum transfer does. Because the diffusion mechanism is less effective at moving species from areas of high concentration to areas of low concentration, as a result, the species concentration declines. The base fluid concentration is found to be dominated by the small suction ($S = 0.5$) rather than the high suction ($S = 5$), and the concentration profile declines as Sc upsurges. Physically, it is connected to the relative thickness of the mass-transfer boundary layer and the hydrodynamic layer. The boundary layer close to the wall may experience fluid flow and mixing due to wall suction. Reduced flow and reduced mixing of the fluid occur when the suction strength is lower. The species-rich fluid is less likely to disperse away from the wall as a result of this decreased mixing. As a result, the species concentration in the fluid is higher overall because it is still higher near the wall.

5. Conclusions

In this investigation of CNT's for Casson fluid in a vertical channel, the main findings are incorporated as:

- This investigation emphasizes the significant role played by MWCNT and SWCNTs for certain key physical parameters. Moreover, it is observed that both the Casson parameter and nanoparticle volume fraction contribute to the acceleration of the flow velocity, regardless of whether SWCNTs or MWCNTs are present.
- In comparison to SWCNTs, MWCNTs are thicker and contain more layers. This structural feature gives MWCNTs a greater aspect ratio, increasing their sensitivity to fluid flow. Because MWCNTs have a bigger surface area, they may interact with the fluid more and are therefore more responsive to changes in velocity. Because of their increased sensitivity, MWCNTs are more suited for precise velocity measurements in channels.
- The temperature generally increases with higher values of the Reynolds number (Re), but shows opposite behaviour with respect to the nanoparticle volume fraction (ϕ).
- Some parameters have notable impacts on shear stress profiles. Increasing the nanoparticle volume fraction (ϕ) and the Casson parameter (γ) enhances the shear stress. Additionally, the impact of Grashof number (Gm) on shear stresses exhibits a reversed behaviour compared to the effect of the magnetic drag force (M).
- With the interesting finding of velocity that SWCNTs at a lower magnetic drag force ($M = 0.2$) are dominant over MWCNTs at a higher magnetic drag force ($M = 2$).
- Moreover, the concentration boundary layer thickness decreases for larger suction values ($S = 5$).

Therefore, the study provides insights into the flow characteristics and behaviour of Casson fluid with CNTs in a vertical channel. The findings contribute to the understanding of nanofluid dynamics and have potential applications in various fields, including nanotechnology, water treatment, conductive plastics, air refinement, mechanical compound materials, sensors, gas storage, and bio-sensors.

References

Casson, N. (1959): A flow equation for pigment-oil suspensions of the printing ink type, Rheology of disperse systems. Pergamon press, London, UK.

Dash, R.K., Mehta, K.N. and Jayaraman, G. (1996): Casson fluid flow in a pipe filled with a homogenous porous medium, Int. J. Eng. Sci., Vol. 34, No. 10, pp. 1145–56.

Hayat, T., Haider, F., Muhammad, T. and Alsaedi, A. (2017): On Darcy-Forchheimer flow of carbon nanotubes due to a rotating disk, Int. J. Heat Mass Transfer, Vol. 112, pp. 248–254. https://dx.doi.org:10.1016/j.ijheatmasstransfer.2017.04.123

Hussain, S. T., Haq, R. U., Khan Z. H. and Nadeem, S. (2016): Water driven flow of carbon nanotubes in a rotating channel, Journal of molecular liquids, Vol. 214, 136–144. https://dx.doi.org: org/10.1016/j.molliq.2015.11.042 0167-7322

Khalid, A., Khan, I., Khan, A., Shaed, S. and Tlilie, I. (2018): Case study of MHD blood flow in a porous medium with CNTS and thermal analysis, Case Studies in Thermal Engineering, Vol. 12, pp. 374–380. https://dx.doi.org: 10.1016/j.csite.2018.04.004

Khan, W. A., Khan, Z. H. and Rahi, M. (2014): Fluid flow and heat transfer of carbon nanotubes along a plate with Navier slip boundary, Appl. Nanosci., Vol. 4, pp. 633–641. https://dx.doi.org:10.1007/s13204-013-0242-9

Kandasamy, R., Muhaimin, I. and Mohammad, R. (2016): Single walled carbon nanotubes on MHD unsteady flow over a porous wedge with thermal radiation with variable stream conditions, Alex. Eng. J., Vol. 55, pp. 275–285. https://dx.doi.org/10.1016/j.aej.2015.10.006 1110-0168

Mayer, J., Mckrell, T. and Grote, K. (2013): The influence of multi-walled carbon nanotubes on single-phase heat transfer and pressure drop characteristics in the transitional flow regime of smooth tubes, Int. J. heat mass transfer, Vol. 58, No. 1-2, pp. 597-609. https://dx.doi:10.1016/j.ijheatmasstransfer.2012.11.074

Pramanik, S. (2014): Casson fluid flow and heat transfer past an exponentially porous stretching surface in presence of thermal radiation. Ain Shams Engineering Journal, Vol. 5, pp. 205–212. https://dx.doi.org:/10.1016/j.asej.2013.05.003

Xue, Q. (2005): Model for thermal conductivity of carbon nanotube-based composites, Phys. B Condense Matter, Vol. 368, pp. 302–307. https://dx.doi.org: 10.1016/j.physb.2005.07.024

Xie, H., Lee, H. Youn, W. and Choi, M. (2003): Nanofluids containing multiwalled carbon nanotubes and their enhanced thermal conductivities, Journal of Applied Physics, Vol. 94, No. 8, pp. 4967–4971.

Xuan, Y., Li, Q. and Hu, W. (2003): Aggregation structure and thermal conductivity of nanofluids. AIChE J., Vol. 49, pp. 1038-1043. https://dx.doi.org: 10.1002/aic.690490420

Aman, S., Khan, I., Ismail, Z., Salleh, M. Z. and Al-Mdalla, Q.M. (2017a): Heat transfer enhancement in free convection flow of CNTs Maxwell nanofluids with four different types of molecular liquid. Sci. Rep., Vol. 7, pp. 2445. https://dx.doi: 10.1038/s41598-017-01358-3

Asma, K., Khan, I., Arshad, K. and Sharidan, S. (2015): Unsteady MHD free convection flow of Casson fluid past over an oscillating vertical plate embedded in a porous medium, Engineering Science and technology, Vol. 18, pp. 309–317. https://dx.doi.org/10.1016/j.jestch.2014.12.006 2215-0986

Aman, S., Khan, I., Ismail, Z., Salleh, M. Z., Alshomrani, A. S. and Alghamdi, M. S. (2017b): Magnetic field effect on Poiseuille flow and heat transfer of carbon nanotubes along a vertical channel filled with Casson fluid, IP Advance, Vol. 7, 015036, pp. 1-18. https://dx.doi.org: 10.1063/1.4975219

Ahmed, S. (2009): Three-dimensional Channel flow through a porous medium, Bulletin of Calcutta Mathematical Society, Vol. 101, No. 5, pp. 503-514.

Maxwell, J.C. and Thompson, J.J. (1904): A Treatise on Electricity and Magnetism, Oxford University Press: Oxford, UK.

Brinkman, H.C. and Luis M. (1952): The viscosity of concentrated suspensions and solutions. J. Chem. Phys., Vol. 20, pp. 571.

Beg, O. Anwar, Zueco, Joaquin and Takhar, H.S., (2009): Unsteady magnetohydrodynamic Hartmann Couette flow and heat transfer in a Darcian channel with Hall current, ion slip, viscous and Joule heating effects: Network numerical solutions. Communications in Nonlinear Science and Numerical Simulation, Vol. 14, No. 4, pp. 1082-1097. https://dx.doi.org: 10.1016/j.cnsns.2008.03.015

Hazarika, S., Ahmed, S. Chamkha, A. J. (2023): Heat Transfer of Casson Fluid in Poiseuille Flow of Carbon Nanotubes: A Power Series Approach, Journal of Nanofluids, Vol. 12, pp. 1–9. https://dx.doi:10.1166/jon.2023.1995

Raza, J., Mebarek-Oudina, F. and Chamkha, A.J. (2019): Magnetohydrodynamic flow of molybdenum disulfide nanofluid in a channel with shape effects, Multidiscipline Modeling in Materials and Structures, Vol. 15 No. 4, pp. 737-757. https://doi.org/10.1108/MMMS-07-2018-0133

Chamkha, A. J., Dogonchi, A. S., Ganji, D. D. (2019): Magneto-hydrodynamic flow and heat transfer of a hybrid nanofluid in a rotating system among two surfaces in the presence of thermal radiation and Joule heating, AIP Advances, Vol 9, 025103. https://doi.org/10.1063/1.5086247

Menni, Y., Chamkha, A.J., Massarotti, N., Ameur, H., Kaid, N. and Bensafi, M. (2020): Hydrodynamic and thermal analysis of water, ethylene glycol and water-ethylene glycol as base fluids dispersed by aluminum oxide nano-sized solid particles, International Journal of Numerical Methods for Heat & Fluid Flow, Vol. 30 No. 9, pp. 4349-4386. https://doi.org/10.1108/HFF-10-2019-0739

Selimefendigil, F., Öztop, H.F. and Chamkha, A.J. (2020): Role of magnetic field on forced convection of nanofluid in a branching channel, International Journal of Numerical Methods for Heat & Fluid Flow, Vol. 30 No. 4, pp. 1755-1772. https://doi.org/10.1108/HFF-10-2018-0568

Selimefendigil, F. and Chamkha, A.J. (2020): MHD mixed convection of nanofluid in a three-dimensional vented cavity with surface corrugation and inner rotating cylinder, International Journal of Numerical Methods for Heat & Fluid Flow, Vol. 30 No. 4, pp. 1637-1660. https://doi.org/10.1108/HFF-10-2018-0566

Hazarika, S. and Ahmed, S. (2021): Material behaviour in micropolar fluid of Brownian motion over a stretchable disk with application of thermophoretic forces and diffusion-thermo, Journal of Naval Architecture and Marine Engineering, Vol. 18, No. 1, pp. 25–38. https://doi.org/10.3329/jname.v18i1.52518

Hazarika, S., Ahmed, S., Chamkha, A. J. (2021): Investigation of Nanoparticles Cu, Ag and Fe_3O_4 on Thermophoresis and Viscous Dissipation of MHD Nanofluid over a Stretching Sheet in a Porous Regime: A Numerical Modelling, Mathematics and Computers in Simulation, Vol. 182, pp. 819-837. https://doi.org/10.1016/j.matcom.2020.12.005

Hazarika, S. Ahmed, S. (2022): Numerical simulation on *Cu–H_2O* nanofluid of destructive and generative reactions in a Darcian medium: application of wall suction and blowing, Waves in Random and Complex Media, pp. 1-21. https://doi.org/10.1080/17455030.2022.2139423

Appendix

$$\phi_1 = (1-\phi) + \phi\frac{\rho_{CNT}}{\rho_f}, \quad \phi_2 = \frac{1}{(1-\phi)^{2.5}}, \quad \phi_3 = 1 + \frac{3(\sigma-1)\phi}{(\sigma+2)-(\sigma-1)\phi},$$

$$\phi_4 = (1-\phi) + \phi\frac{(\rho\beta)_{CNT}}{(\rho\beta)_f}, \quad \phi_5 = (1-\phi) + \phi\frac{\left((\rho C_p\right)_{CNT}}{\left((\rho C_p\right)_f}, \quad a_0 = \phi_1 Re,$$

$$a_1 = \phi_2\left(1+\frac{1}{\gamma}\right), a_2 = M^2\phi_3, \quad a_3 = \phi_4 Gr, \quad a_4 = \phi_4 Gm, \quad a_9 = Sa_0,$$

$$b_0 = \frac{\phi_5 Pe}{\lambda_n}, \quad b_1 = \frac{R^2}{\lambda_n}, \quad a_5 = \frac{a_2}{a_1}, \quad a_6 = \frac{a_3}{a_1}, a_7 = \frac{a_4}{a_1}, \quad a_8 = \frac{a_0 i\omega + a_2}{a_1},$$

$$b_2 = Sb_0, \quad b_3 = (b_0 i\omega - b_1), \quad d_0 = S.Sc, \quad d_1 = i\omega Sc, \quad \lambda_1 = \frac{\lambda}{a_1},$$

$$A = \frac{e^{-d_0}}{e^{-d_0}-1}, \quad n_2 = \frac{b_2+\sqrt{b_2^2-4b_1}}{2}, \quad B = \frac{e^{n_2}}{e^{n_2}-e^{-n_2}}, \quad n_3 = \frac{a_9+\sqrt{a_9^2+4a_5}}{2},$$

$$p_1 = \frac{-Ba_6}{n_2^2-a_9n_2-a_5}, p_2 = \frac{-a_6(1-B)}{n_2^2+a_9n_2-a_5}, p_3 = \frac{Aa_7}{a_5}, \quad p_4 = \frac{a_7(1-A)}{d_0^2-a_9d_0-a_5},$$

$$p_5 = p_2 + p_4 - p_1 - p_3, \quad n_4 = \frac{a_9+\sqrt{a_9^2+4a_8}}{2}, \quad E = \left(\frac{1-e^{-n_4}}{e^{n_4}-e^{-n_4}}\right)\frac{\lambda_1}{a_8},$$

$$D = \frac{1}{e^{n_3}-e^{-n_3}}\{p_2e^{n_2} + p_4e^{-d_0} - p_5e^{-n_3} - p_1e^{-n_2} - p_3\}.$$